Quantum Drift Diffusion and Quantum Energy Simulation of Nanowire Transistors

O. Badami, N.Kumar, D. Saha, S. Ganguly
CEN & Department of Electrical Engineering,
Indian Institute of Technology Bombay,
Mumbai 400076, India.
swaroop.ganguly@gmail.com.

Abstract— **In this paper we have developed a quantum drift-diffusion (QDD) and quantum energy-balance (QEB) based simulator for scaled nanowire devices. Solving the QDD+QEB along the length of the wire together with Schrodinger equation across its cross-section allows us to take into account the energy quantization, velocity overshoot and tunneling. In addition, the Schrodinger equation reduces the dimensionality of the transport equations. We also discuss the discretization scheme and numerical implementation of QDD and QEB. This was then applied to a specific case of nanowire MOSFET.**

Keywords-Quantum Drift Diffusion; Quantum Energy Balance; Generalized Scharfetter-Gummel;

I. INTRODUCTION

Over the past few years, the search for alternatives to bulk planar MOSFET has intensified and multi-gate MOSFETs have appeared to be the most promising candidates because of excellent electrostatic integrity. Because of extremely small cross-sectional area and channel length, the characteristics of these devices are strongly influenced by the structural confinement across the channel and quantum and non-local effects like tunneling and velocity overshoot along the transport direction. In order to capture these effects in a framework, that preserves the connection to the familiar drift-diffusion, we have developed a simulator for nanowire devices in which we solve the Quantum Drift-Diffusion (QDD) [1] and Quantum Energy Balance (QEB).

In this work, we have extended the technique of Baccarrani [1] to Quantum Energy Balance and this converted 3D Quantum Energy Balance (2D for cylindrical geometry using the symmetry along φ) to 1D and thus reducing the computational effort without missing out on most of the essential physics.

II. FORMALISM

The energy balance equations can be obtained from the hydrodynamic equations under suitable approximations [2]. In this work, we have solved QDD and QEB. The quantum counter parts of classical drift diffusion and energy balance differ only by correction factors to the electrostatic potential ($-\frac{\hbar^2}{2m^*}\frac{1}{\sqrt{n}}\Delta\sqrt{n}$) and energy terms ($-\frac{\hbar^2}{24m^*q}\Delta\log(n)$). However, by solving Schrodinger equation across the channel, we can replace the sum of the Bohm and electrostatic potential by the sub-band potential [1]. This avoids the difficult boundary condition of the Bohm potential at the semiconductor-oxide or semiconductor-air interface and the use of an empirical constant [1].

Solving the Schrodinger equation across the cross-section reduces the dimensionality of the equations as the sub-band energy is invariant is the directions other than along the length. Solving the Schrodinger equation across the channel gives us an additional advantage to incorporate any number of sub-band energies whereas in case of density gradient method (addition of the Bohm potential to the electrostatic potential) one considers the first sub-band only [1]. This becomes important when higher sub-bands make significant contributions to the total electron density. Since the doping has n+-n-n+ structure, we have solved the equations for electrons only. The equations are stated below

$$\left(\frac{d^2}{dr^2}+\frac{1}{r}\frac{d}{dr}\right)V = -\frac{q}{\epsilon_{SI}}(N_D-n) \tag{1}$$

$$\frac{-\hbar^2}{2m^*}\left(\frac{d^2}{dr^2}+\frac{1}{r}\frac{d}{dr}+\frac{l^2}{r^2}\right)\psi - qV\psi = E_{sb}\psi \tag{2}$$

$$\frac{dJ}{dz}=0 \tag{3}$$

$$J=\sum_{sb} n_{sb}\mu_{sb}\frac{dE_{sb}}{dz}+k_B\frac{d(n_{sb}T)}{dz} \tag{4}$$

$$\frac{dS}{dz}=\sum_{sb}\frac{J_{sb}}{q}\frac{dE_{sb}}{dz}-\frac{3}{2}n_{sb}k_B\frac{T-T_l}{\tau_\epsilon} \tag{5}$$

$$S=\sum_{sb}\frac{k_B\delta T n_{sb}\mu_{sb}}{-q}\frac{dE_{sb}}{dz}+\frac{k_B^2T^2}{q}\mu_{sb}\delta\frac{dn_{sb}}{dz}-\frac{k_B^2T}{q}(\delta+\Delta)\frac{dT}{dz}n_{sb}\mu_{sb} \tag{6}$$

where V is the electrostatic potential, m^* is the effective mass, ψ is the wave function, E_{sb} is the sub-band energy, l is the order of the Bessel function, T is the electron temperature, τ_ϵ is the energy relaxation time for an electron, n_{sb} (m^{-1}) is the electron concentration in a particular sub-band energy and n (m^{-3}) is the total electron density. $\delta(T)$ and $\Delta(T)$ are $\frac{<\tau\epsilon^2>}{<\tau\epsilon>}$ and $\frac{1}{(Tk_B)^2}[\frac{<\tau\epsilon^3>}{<\tau\epsilon>}-(\frac{<\tau\epsilon^2>}{<\tau\epsilon>})^2]$ respectively as obtained by Stratton [3]. V is independent of the angle (φ) because of the symmetry.

 ISBN 978-0-615-71756-2

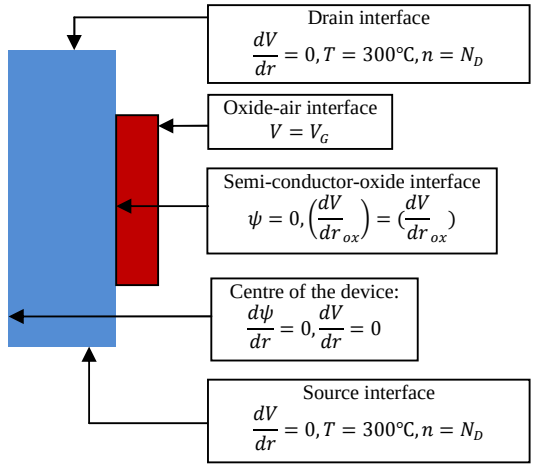

Figure. 1. Boundary conditions used in the simulation

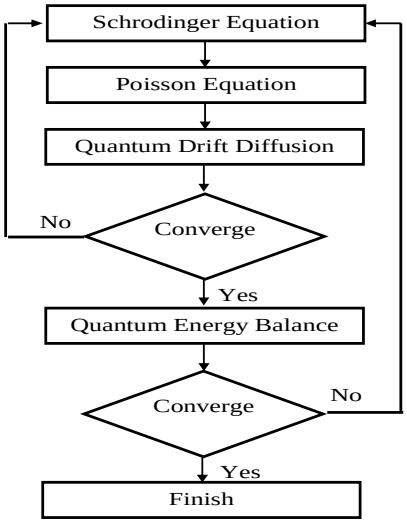

Figure 2. Flowchart for simulation of QEB for one bias point.

The corrections to the energy term $\left(\frac{\hbar^2}{24m^*q}\Delta\log(n)\right)$ is neglected. The closure for the above equations was provided by Fourier's law $(-\kappa(T_n)\Delta T_n)$ and $\kappa(T_n)$ can be obtained by using Weidemann-Franz law.

III. DISCRETIZATION AND SIMULATION

All the equations were discretized by using the finite difference method. For discretizing the transport equations, Generalized Scarfetter-Gummel scheme as derived by Tang [4] was used. Equations 4 and 6 are first converted into 1st order linear differential equations for electron density, n_{sb}. Then under the assumptions that V, T vary linearly and S is almost constant between two successive nodes, we can determine the integrating factors for QDD and QEB. This leads to the following discretized equation.

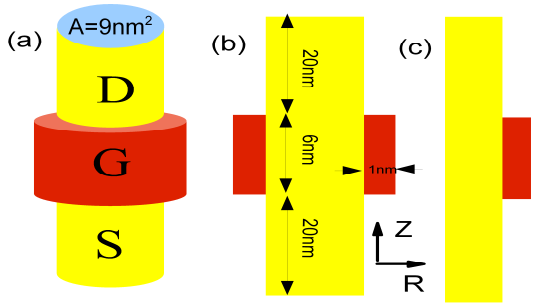

Figure. 3. (a) Schematic of the nanowire transistor. (b) Structure obtained exploiting cylindrical symmetry, and, (c) half-plane fundamental domain used for simulation.

$$J_{i+\frac{1}{2}} = \left(\frac{k_B(T_{i+1}-T_i)}{x_{i+1}-x_i} - \frac{Esb_{i+1}-Esb_i}{x_{i+1}-x_i}\right) \frac{\left(\mu n_{i+1}\exp\left(\frac{Esb_{i+1}-Esb_i}{k_B(T_{i+1}-T_i)}\right)\ln\left(\frac{T_{i+1}}{T_i}\right) - \mu n_i\right)}{\exp\left(\frac{Esb_{i+1}-Esb_i}{k_B(T_{i+1}-T_i)}\right)\ln\left(\frac{T_{i+1}}{T_i}\right) - 1}$$

$$S_{i+\frac{1}{2}} = -\frac{k_B}{q}\left(\Delta\frac{k_B(T_{i+1}-T_i)}{x_{i+1}-x_i} - \delta\left(\frac{Esb_{i+1}-Esb_i}{x_{i+1}-x_i}\right)\right) \frac{\left(\mu n_{i+1}T_{i+1}\exp\left(\frac{Esb_{i+1}-Esb_i}{k_B(T_{i+1}-T_i)}\right)\ln\left(\frac{T_{i+1}}{T_i}\right) - \mu n_i T_i\right)}{\exp\left(\frac{Esb_{i+1}-Esb_i}{k_B(T_{i+1}-T_i)}\right)\ln\left(\frac{T_{i+1}}{T_i}\right) - 1}$$

Similarly, we can calculate the expression of $J_{i-\frac{1}{2}}$ and $S_{i-\frac{1}{2}}$ and use equations discretized versions of equations (3) and (5) we can eliminate J and S and calculate n_i and T_i.

Boundary conditions used in the simulation are summarized in Fig. 1. For Poisson equation, Neumann boundary condition was used at the source and the drain edges because using a fixed value of the potential would fix the potential profile and thus the profile of the electron density. Also because of symmetry at the centre of the device the potential was assumed be constant. It is assumed that the Einstein's relationship $\left(\frac{D}{\mu} = \frac{k_BT}{q}\right)$ holds. Laplace equation was used in order to calculate the electric field in the oxide.

Fig. 2 shows the flowchart of the QEB simulation for one bias point. All the equations were solved by Gummel based iterative scheme. Poisson, carrier continuity, and quantum energy balance were solved using LU decomposition method as described in [5]. For faster convergence a relaxation scheme for calculating the electron temperature was implemented $(T^{j+1} = T^j + \alpha(T^{j+1} - T^j))$ where the relaxation parameter α was taken to 0.5and j is the iteration number. It is important to note that the electron density obtained for the carrier continuity equation has units of m^{-1} while that in the Poisson equation has

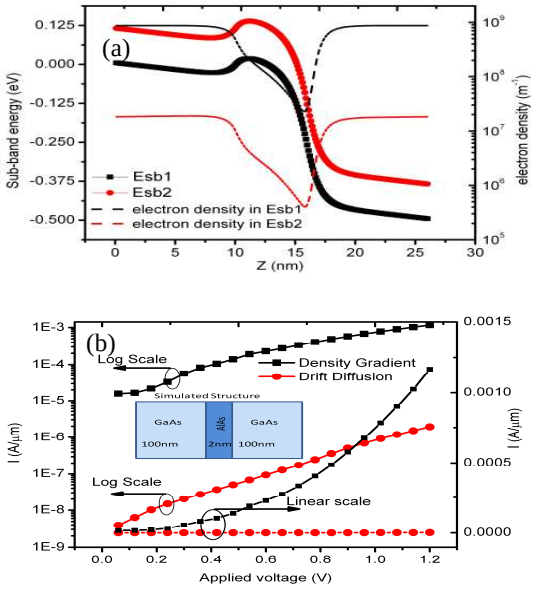

Figure 4. (a) Comparison of the electron density in the 1st and 2nd sub-bands. Similar results are also obtained in [1]. (b) Results from Sentaurus indicating tunneling effect through a single barrier.

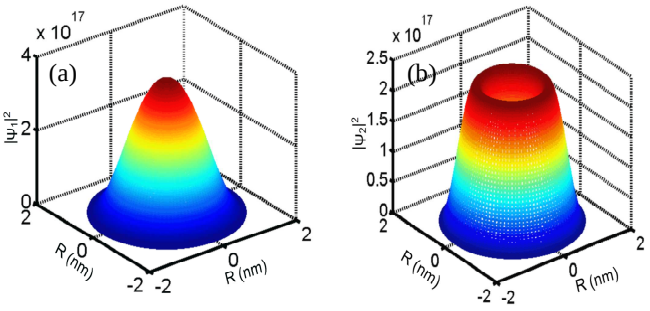

Figure 5. Probability density of the electrons in the 1st (a) and 2nd (b) sub-band.

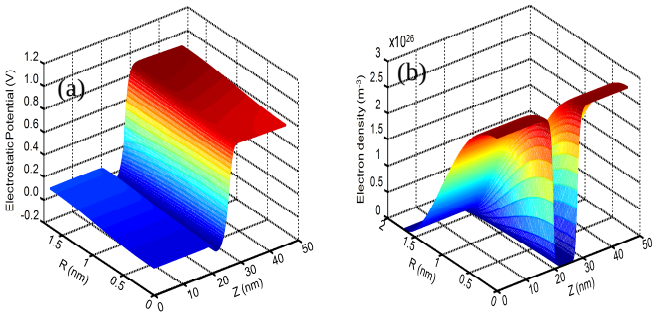

Figure 6. (a) Electron density and (b) Potential profile in the nanowire transistor for Vd=0.1V and Vg=0.1V

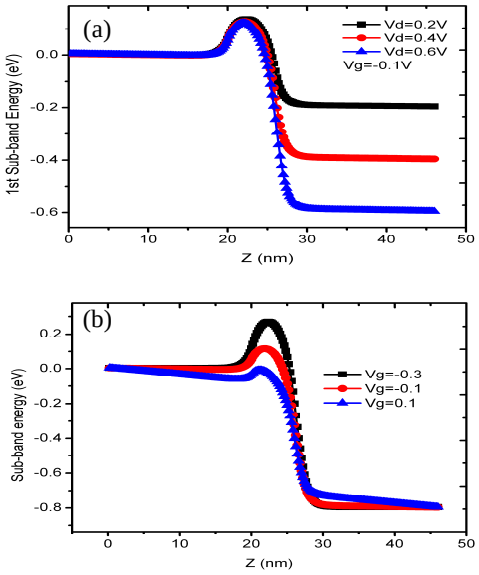

Figure. 7. Variation in the 1st sub-band along Z for different values of (a) gate and (b) drain voltage.

units of m^{-3}. The transformation of the carrier density from per unit length to per unit volume can be done by [6] $n = \sum_{sb} n_{sb} |\psi_{sb}|^2$. This can be explained as n_{sb} is the total electron density in a particular cross-section and sub-band. The probability distribution of the electrons in the cross-section is given by $|\psi_{sb}|^2$. All the simulations were done with constant μ=500 cm^2/V-sec and Δ=δ=2.

Fig. 3 shows the schematic of a nanowire transistor. By exploiting the symmetries of the cylindrical nanowire, the actual simulation domain is shown in the Fig. 3(c). This significantly reduces the computational effort. It is shown in [7] that for extremely scaled geometries, electron density is same irrespective of whether the cross-section is circular or square. For verification of the code, a NW-MOSFET structure having the same cross-sectional area as used by [8] was simulated the results shown in Fig. 4(a) are in close agreement with what have been obtained there. Fig. 4(b) shows a TCAD simulation [9] illustrating the capability of the density-gradient method, a derivative of QDD, to model tunneling. For the purpose of simulation only one sub-band as the contribution to the electron density and hence the current from the higher sub-bands is negligible (Fig. 4 (a))

IV. NUMERICAL RESULTS

The source and drain doping in the nanowire MOSFET were assumed assumed to be 10^{20} cm^{-3} and intrinsic channel. Fig. 6 shows the electron density and potential profile in the device. As expected, the electron density is maximum in the centre of the device and falls off towards the edges. The plot of the first sub-band energy for different drain and gate bias is shown in Fig. 7 For larger gate bias the increase in the drain current causes significant drop across the source and drain regions (Fig. 7(b)). Comparison of Id-Vd and Id-Vg characteristics due to QDD and QEB is shown in the Fig.8. A sub-threshold swing of about 80mV/dec is observed. The characteristics calculated by QDD and QEB differ significantly in both the off current and output resistance which are important to digital and analog applications

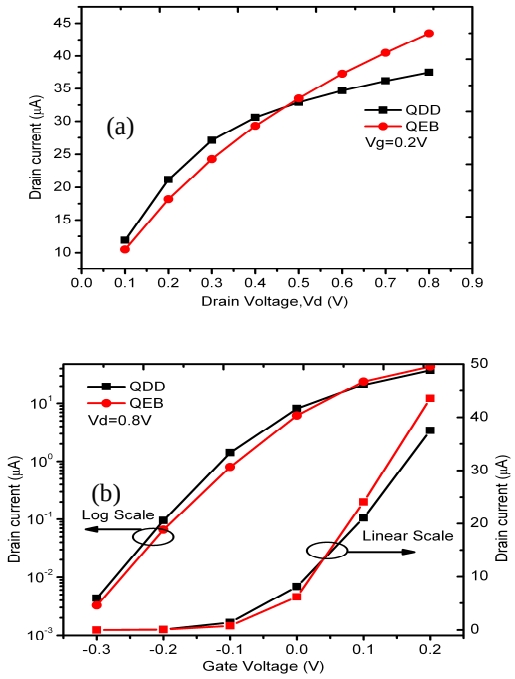

Figure 8. Comparison of (a) Id-Vd and (b) Id-Vg with QEB and QDD.

respectively. The temperature profile in Fig.9 shows electrons heated way above the lattice temperature 300K.

V. CONCLUSION

In this paper, we have described the discretization and numerical implementation of the Schrodinger, Poisson, and 1D transport (QDD+QEB) equations. It was then applied to a nanowire MOSFET. It is noted that there is significant difference between the output and the transfer charateristics of the device obtained from QDD and QEB equations.

.

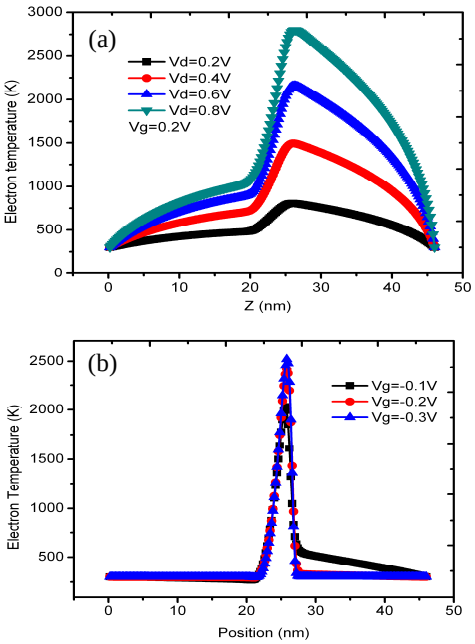

Figure. 9. Electron temperature profile for different (a) drain and (b) gate bias.

REFERENCES

[1] Giorgio Baccarani, Elena Gnani, Antonio Gnudi, Sussana Reggiani and Massimo Rudan, "Theoretical foundations of the quantum drift diffusion and density gradient model," Solid State Electronics, vol. 52, pp. 526–532, April 2008.

[2] Tibor Grasser, Ting-Wei Tang, Hans Kosina and Siegfried Selberherr, "A review of Hydrodynamic and energy transport models for semiconductor device simulation." Proceedings of IEEE, vol. 91, pp251-274, February 2008.

[3] R.Stratton, "Diffusion of hot and cold electrons in the semiconductor barriers," Phys. Rev., vol. 126, pp. 2002–2014, June 1962.

[4] Ting-Wei Tang, "Exetension of Scharfetter-Gummel algorith, to energy balance equation," IEEE Transactions on Electron Devices, vol. 31, pp. 1912-1914, December 1984.

[5] Dragica Vasileska, Stephen Goodnick, Gerhard Klimeck, Computational Electronics Semiclassical and Quantum Device Modeling and Simulation, CRC Press, Jun 2010, pp.177.

[6] Gianluca Fiori and Giuseppe Iannnaccone, "Three dimensional simulation of one dimensional transport in silicon nanowire transistors," IEEE Transactions on Nanotechnology, vol.6, pp. 524–529, September 2007.

[7] Elena Gnani, et al "Band-structure effects in ultra scaled silicon nanowires," IEEE Transactions on Electron Devices, vol. 54, pp. 2243–2254, September 2007.

[8] Yoshihiro Yamada, Hideaki Tsuchiya and Matsuto Ogawa, "Quantum Transport Simulation of Silicon-Nanowire Transistors Based on Direct Solution Approach of the Wigner Transport Equation," IEEE Transactions on Electron Devices VOL: 56, 1396-1401, July 2009.

[9] S-Device Manual Version F 2011.09